https://doi.org/10.5194/egusphere-2026-534
Preprint. Discussion started: 29 April 2026

Ocean Model Analysis and Prediction System version 4.1i (OceanMAPSv4p1i)

Prasanth Divakaran[1], Pavel Sakov[1], Gary Brassington[1], Xinmei Huang[2]

[1]Research Program, Science and Innovations Group, Bureau of Meterology, Docklands, 3008, Australia
[2]Research to Operations, Science and Innovations Group, Bureau of Meterology, Docklands, 3008, Australia
Correspondence to: Prasanth Divakaran (prasanth.divakaran@bom.gov.au)

Abstract. The Ocean Model Analysis and Prediction System (OceanMAPS) is a short-range, near-global, eddy-resolving ocean forecasting system developed at the Bureau of Meteorology. OceanMAPS runs daily, producing 7-day forecasts of 3D prognostic fields of ocean currents, temperature, salinity and sea level anomalies (SLA's). OceanMAPS is based on MOM5 ocean general circulation model and uses EnKF-C software for data assimilation. Consistent with the previous version of OceanMAPS, version v4p1i (OceanMAPSv4p1i), is based on a hybrid Ensemble Kalman Filter with 48 dynamic and 144 static members. However, OceanMAPSv4p1i employs a 1-day analysis cycle in place of the 3-day cycle in OceanMAPSv4p0i. OceanMAPSv4p1i utilises an asynchronous data assimilation of observations, including Sea Surface Temperature (SST; 2-hourly), SLA (12-hourly), and temperature and salinity profiles (daily). OceanMAPSv4p1i produces better performance in forecast skill and mean absolute error scores in Sea Level Anomaly, Sea Surface Temperature and subsurface Temperature. Improvements gained are greater in surface fields, such as sea level anomaly and sea surface temperature, which have less persistence and a greater tendency. A reduction of ~10 % in SST errors and a ~7-8 % reduction in SLA errors is demonstrated in forecast stats. OceanMAPSv4p1i forecasts also better represent mesoscale ocean eddies.

1 Introduction

Operational ocean forecasting started in the mid-1990s following the launch of satellite altimetry (Dombrowsky, 2009). Ocean forecasting system development found impetus from scientific improvements during the past decades, primarily in the progress achieved in satellite measurement of the sea surface, the development of eddy-permitting and eddy-resolving general circulation models and the evolution of data assimilation techniques to combine observations and ocean models to produce reliable forecast products. The period also saw excellent achievements in sustained ocean observations under the Global Ocean Observing System (GOOS) framework (Nowlin Jr, 1996; Moltmann et al., 2019), especially in increased high-quality subsurface ocean observations, along with accurate global sea surface temperature (SST) (errors <1 ºC) and sea level measurements (<4 cm error) (Kilpatrick et al., 2001; Shum et al., 1995). This was complemented by advances in supercomputing technology, allowing the development and operational implementation of eddy-resolving (~10 km) basin-scale ocean circulation models. To accelerate progress and coordinate efforts within the broader operational oceanography community, the Global Ocean Data Assimilation Experiment (GODAE) was established in 1997 (Smith and Lefebvre, 1997; IGST, 2000). The strategic aim of GODAE was to demonstrate the feasibility and utility of global

https://doi.org/10.5194/egusphere-2026-534
Preprint. Discussion started: 29 April 2026

ocean monitoring and forecasting in eddy-resolving scales on daily-weekly timescales and assist the infrastructure development for global operational oceanography (IGST, 2000; Bell et al., 2009). The GODAE program eventually ended in 2008 and was replaced by GODAE Ocean View (GOV), and since 2019, OceanPredict (www.oceanpredict.org). GODAE has made a significant impact on global ocean forecast system capability. Since then, global modelling and data assimilation systems have been progressively developed, implemented, intercompared and verified (Brassington, 2017; Divakaran et al., 2015; Ryan et al., 2015; Hernandez et al., 2015; Dombrowsky et al., 2009; Cummings et al., 2009).

Coinciding with the global trend towards the development of ocean forecasting systems mentioned above, the Australian government, through a partnership with the Bureau of Meteorology (BoM), CSIRO, and the Royal Australian Navy, initiated the BLUElink project in 2004 to develop Australia's first ocean forecasting system. The Ocean Model, Analysis, and Prediction System (OceanMAPS; Bureau of Meteorology, 2007; Brassington et al., 2006, 2007) was implemented operationally in August 2007 (Bureau of Meteorology, 2007). OceanMAPS produces daily 7-day forecasts of the surface and subsurface ocean state and circulation, focusing on resolving ocean weather (mesoscale ocean features) around Australia. OceanMAPS continued to be developed through the Bluelink partnership follow-on projects, which delivered a wide range of benefits to the Australian community (Schiller et al., 2019). OceanMAPS has subsequently undergone several significant upgrades whilst maintaining continual service. A major upgrade to version 2.0 (OceanMAPSv2; Brassington et al., 2012) was introduced on 8 November 2011 (Bureau of Meteorology, 2011), followed by a later update (OceanMAPSv3p0) on 13 April 2016 (Bureau of Meteorology, 2017). OceanMAPSv2 increased the vertical resolution and introduced a multi-cycle time-lagged ensemble design (Brassington, 2013), and OceanMAPSv3p0 extended the eddy-resolving (1/10°) horizontal resolution to all longitudes and latitudes between 75° S-75° N. The system was further upgraded to version 3.1 on June 22, 2016, version 3.2 on July 2, 2019, and version 3.3 on May 26, 2020. The atmospheric forcing inputs were replaced by the Australian Community Climate and Earth System Simulator – Global v2 model (ACCESS-G2; Bureau of Meteorology, 2016) in version 3.1, and the ocean model was updated to the latest stable MOM5 in version 3.2. In version 3.3, ACCESS-G3 (G3; Bureau of Meteorology, 2019) replaced the atmospheric forcing inputs and introduced a new surface fluxes scheme (Huang et al., 2020). OceanMAPS underwent a minor upgrade (OceanMAPSv3p4) in May 2021, focusing on modifications to the data assimilation scheme. OceanMAPSv3p4 implemented a two-stage data assimilation process, utilising 144 static high-resolution and 480 coarse-resolution members in the first and second stages, respectively (Chamberlain et al., 2021; Huang et al., 2021).

Specifically, regarding the data assimilation (DA) strategy, up to and including version 3.4, OceanMAPS utilised the ensemble optimal interpolation (EnOI) scheme based on static ensemble members (Oke et al., 2010). In earlier OceanMAPS versions, up to v2.0, the data assimilation was based on the Bluelink Data Assimilation System (BODAS) (Oke et al., 2008), developed in-house by CSIRO through the Bluelink partnership. Starting from version 3.0, OceanMAPS adopted the public software EnKF-C (Ensemble Kalman Filter coded in the C programming language) (Sakov, 2014) developed at BoM, which provided a redesign to improve the computational performance and potential extension to the Ensemble Kalman Filter. The EnOI approach, which utilises quasi-dynamically consistent, stationary background error covariances, offers both forecast skill and

https://doi.org/10.5194/egusphere-2026-534
Preprint. Discussion started: 29 April 2026

computational efficiency for eddy-resolved ocean forecast systems. EnOI is an effective strategy for many applications being cheaper to run and can be a good fit for assimilation systems, especially based on sparse observations relative to the scales represented by the model (Oke et al., 2010). However, due to the static nature of ensembles in EnOI, they do not adequately represent the state-dependent, time-evolving error covariances of the system, leading to dynamic inconsistencies in updated fields (Brassington et al., 2023). Unbalanced updates can lead to factitious ageostrophic waves and unrealistic vertical velocities (Li and Toumi, 2017; Pilo et al., 2018) in the forecast system. An Ensemble Kalman Filter (EnKF) method, with a sufficiently large ensemble size, is designed to capture the system's temporal and spatial variability, providing better-balanced increments than an EnOI system (Brassington et al., 2023). Furthermore, the current increase in computing capacity enables us to utilise more advanced data assimilation techniques (e.g., EnKF and 4D variational) in operational ocean forecasting, rather than the suboptimal assimilation systems (e.g., EnOI, 3D variational, reduced Kalman Filter) that have been popular in recent decades. Starting from version 4.0i, OceanMAPS employs a hybrid EnKF/EnOI data assimilation method (Counillon et al., 2009; Sakov, 2014; Brassington et al., 2023). This system comprises 48 dynamic and 144 static members, with a sequential analysis cycle of 3 days. OceanMAPSv4p0i was the first eddy-resolving global EnKF operational ocean forecasting system. In this paper, we discuss an upgrade to the Bureau's ocean forecast system, OceanMAPS version 4.1i (OceanMAPSv4p1i), and the improvements in forecast quality it brings.

The paper is organised as follows. In Section 2, we describe the components of the system and outline the system layout; in Section 3, we compare the system's performance using data from the parallel forecast run. The conclusion and discussion are presented in Section 4.

2 System Description

The OceanMAPS ocean prediction system comprises ocean observations, an ocean general circulation model, an ocean data assimilation system that merges observations with a model background, and forcing for deterministic integration (Brassington et al., 2012). The main components of OceanMAPSv4p1i are the observation and quality control system, the Ocean Forecast Australia Model version 3 (OFAM 3; Oke et al., 2013), the EnKF-C data assimilation system, and surface atmospheric variables (such as radiative fluxes, air temperature, specific humidity and winds) from ACCESS-G (Puri et al., 2013) for bulk flux calculation.

2.1 Observational Inputs

The observational products used in OceanMAPSv4p1i remain the same as in OceanMAPSv4p0i (Brassington et al., 2023). OceanMAPS assimilates real-time ocean observations, including satellite observations of sea-surface temperature (SST), sea-level anomalies (SLA), and *in situ* temperature and salinity profiles. Below is a short description of each platform.

2.1.1 In-situ profiles

https://doi.org/10.5194/egusphere-2026-534
Preprint. Discussion started: 29 April 2026

OceanMAPS utilises *in situ* data collected through the ship-of-opportunity program (SOOP), the Argo project, and moored buoys. SOOP is mainly comprised of real-time measurements of eXpendable Bathy-Thermograph (XBT) and Conductivity-Temperature-Depth (CTD) profiles. Argo is a global array of free-drifting profile floats designed to measure the temperature and salinity of the upper 2000 m of the ocean (Roemmich et al., 2001). All the real-time observations are downloaded in-house through the WMO Global Telecommunication System (GTS). However, the Argo observations are retrieved by a network of Data Assembly Centres (DAC's), which are responsible for performing an automatic quality control before uploading the processed observations to both the GTS with a low latency and the two Global DACs (USGODAE and Coriolis) with a typical latency of approximately 2-3 days. BoM has adopted the strategy of downloading Argo data from the GDACs and performing a duplicate checking procedure to create a superset of the best-quality profiles (Brassington et al., 2012). When this strategy was first implemented, the Argo data on the GTS were based on a thinned set of observations, and the GDACs had a complete set of each profile. Since that time, Argo messages have been upgraded to BUFR, providing complete profiles and quality flags. The justification for the retention of this approach is the latency of the different systems operating in different time zones.

2.1.2 Sea surface temperature

All satellite sea surface temperature (SST) observations assimilated into OceanMAPS used data formats specified by the Group for High-Resolution SST (GHRSST; GHRSST Science Team, 2012) with the current version 2.0 revision 5. OceanMAPS uses either Level 2 pre-processed (L2P) geolocated swath or Level 3 Uncollated (L3U) gridded netCDF4 files. OceanMAPS ingests SST observations from the Advanced Microwave Scanning Radiometer 2 (AMSR-2), U.S. Naval Oceanographic Office's (NAVOCEANO) Global Area Coverage (GAC) Advanced Very High Radiometer (AVHRR) L2P SST and Suomi NPP and NOAA-20 VIIRS L3U SST.

The NAVOCEANO GAC AVHRR L2P SST data from the Naval Oceanographic Office are made available under the Multi-sensor Improved Sea Surface Temperature (MISST) project sponsored by the Office of Naval Research (ONR). The VIIRS Level 3 Uncollated (L3U) data are provided by the National Oceanic and Atmospheric Administration (NOAA). AMSR-2 L2P SST data are provided by the Japan Aerospace Exploration Agency (JAXA) Earth Observation Research Centre (EORC). All SST data are obtained daily from external servers, then processed and reformatted for ocean data assimilation. Only quality level 5 (best quality) SST observations are used. All SST data are corrected for bias by subtracting sses_bias (derived by each data provider using matchups with drifting buoy and tropical mooring SST).

2.1.3 Satellite altimetry

OceanMAPSv4p1i makes use of six satellite altimeters available for operational oceanography: Jason-3, Sentinel (3A, 3B, 6A), CryoSat-2 and satellite with Argos and ALtika (SARAL). OceanMAPS does not process the raw satellite altimetry observations. The altimetry data are retrieved from a common source and in the standard data format from the Radar Altimeter Database System (RADS), developed by the Delft Institute for Earth-Oriented Space Research and the NOAA Laboratory for Satellite Altimetry (Scharroo et al., 2016), to ensure consistent data processing. Due to the time required to calculate the sea level accurately, there is a delay of 1-2 days in the

https://doi.org/10.5194/egusphere-2026-534
Preprint. Discussion started: 29 April 2026

provision of the data from the time of measurement. The altimetry data are processed with quality control at BoM before being used for ocean data assimilation.

2.2 Atmospheric forcing

Atmospheric forcing input into OceanMAPS comes from deterministic global atmospheric forecast outputs from the Bureau's operational numerical weather prediction system, ACCESS-G. The current version of ACCESS-G is Australian Parallel Suit 4 (commonly referred to as "APS4" or "G4"), which was operationalised in June 2025. ACCESS-G is based on the UK Met Office's Unified Model/Variational Assimilation/Observations processing/Land Surface Data Assimilation (UM/VAR/OPS/SURF) systems (Walters et al., 2017; Clayton et al., 2013). The ACCESS-G4 and ACCESS-G3 (previous NWP system) deterministic model have the same horizontal resolution of ~12 km. Both produces high temporal resolution in model outputs, including several single-level fields written out every 10 minutes up to 240 hours (Bureau of Meteorology, 2019). OceanMAPS is forced by 1-hourly deterministic forecast outputs of ACCESS-G. OceanMAPS uses a "bulk flux" method to derive surface exchanges (Large and Yeager, 2004) using atmospheric forcing inputs from G3/G4, namely, surface net shortwave radiation, surface downward longwave radiation, precipitation rate and first model level (10m) variables like air temperature, specific humidity, meridional and zonal wind vectors. The penetrating shortwave heat flux is applied using the quantification heat flux of the upper ocean and bio-optical feedback for visible and near-infrared using Chlorophyll data (Manizza et al. 2005). To generate spread between individual ensemble member ocean model runs for EnKF Ocean Data Assimilation System, a random number multiplication factor is applied to each input atmospheric flux variable. The scale of randomness for the deterministic forecast input fluxes is presented in Table 1. However, ensemble member-001 is chosen to run without modification to the actual surface flux from the atmospheric model in order to generate a single deterministic forecast that closely resembles EnOI forecast products from previous OceanMAPS systems based on the Ensemble Optimal Interpolation (EnOI) method. The operational version of OceanMAPSv4p1i is currently running with ACCESS-G4, however, the study presented here is based on pre-operational forecast trails conducted with ACCESS-G3.

2.3 Data Assimilation

Starting from version 4.0i, OceanMAPS forecasting system DA is based on the ensemble Kalman Filter (EnKF; Evenson 1994), which uses an approximation of the ensemble square root filter (Tippett et al., 2003) referred to as the deterministic EnKF (DEnKF; Sakov and Oke, 2008). Specifically, OceanMAPS uses a hybrid EnKF/EnOI method in ocean forecasting. In the hybrid EnKF, the forecast state error covariances (P) is equal to the sum of "dynamic covariances" (P^{dyn}) carried by the EnKF ensemble and "static" covariances (P^{stat}) carried by a pre-defined ensemble of anomalies (Sakov, 2014).

$$P^f = P^{dyn} + \gamma P^{stat} \quad (1)$$

where,

https://doi.org/10.5194/egusphere-2026-534
Preprint. Discussion started: 29 April 2026

$$P^{dyn} = \frac{1}{m_{dyn}-1} A^{dyn}(A^{dyn})^T \quad (2)$$

$$P^{stat} = \frac{1}{m_{stat}-1} A^{stat}(A^{stat})^T \quad (3)$$

where A^{dyn} is the ensemble of dynamic anomalies of size m_{dyn}, and A^{stat} is the ensemble of static anomalies of size m_{stat}. γ is a constant that can assume any values <=1, in OceanMAPSv4p0i/v4p1i, $\gamma = 0.25$. The EnKF-C user manual (Sakov, 2014) provides more information on hybrid EnKF data assimilation.

OceanMAPS4p1i uses 48 dynamic ensemble members and 144 static ensemble members. The static ensembles are constructed from climatological anomalies based on a coarse resolution (~1°) global model run. OceanMAPSv4p1i uses a daily DA cycle with a one-day observation window (-1.0-0 days) relative to the analysis date. Previous versions of OceanMAPS (v4p0i and v3.4) implemented a 3-day assimilation cycle with a 3-day observation window (-3.0 to 0 days). OceanMAPSv4p1i also employs two data assimilation rounds per forecast cycle. The first ("best-estimate") is performed 3 days behind real-time, assimilation (BRT) using the 48 hindcasts from the previous forecast cycle. The additional latency maximises the observational data for altimetry and *in situ* profiles. All 48 ensemble members complete a 1-day hindcast to 2 days behind (near) real-time, permitting an additional analysis (NRT) using available observations. This is followed by a set of catch-up hindcasts that runs 2-days to real-time using hindcast atmospheric bulk fluxes. Followed by the forecast run using forecast atmospheric bulk fluxes. Both BRT and NRT use the same data assimilation settings. The observations are assimilated asynchronously (Sakov et al., 2014) for SST, SLA and *in-situ* temperature and salinity. SST observations are assimilated asynchronously in 2-hourly batches, whereas half-daily and daily batching applies to SLA and T/S observations, respectively.

In order to manage the spurious covariances at large distances from the observation due to the small ensemble, the impact of observations is localised by increasing its error variances with distances as the inverse of the Gaspari and Cohn taper function. A localisation radius of 175 km is chosen for SLA observations; SST observations use a localisation of 150 km, whereas, for subsurface observations, the localisation radius is fixed to 450 km. The observation error standard deviation is set to 0.5 K and 0.075 PSU for subsurface temperature and salinity, respectively. SLA and SST observation error variances are obtained from the observation data files.

If multiple observations of each type occur in a grid cell, observations are superobbed by merging spatially close observations before assimilation. In OceanMAPS, superobbing is done at every model grid cell. The observations are merged by averaging their values, coordinates and times with weights inversely proportional to the observation error variance. The observational error variance of a superobservation is set to the inverse of the sum of the inverse observation error variance of the merged observations (Sakov, 2014). A relatively large number of observations belonging to a particular observation type (e.g. SST) can lead to overfitting of that type of observation. In order to effectively tackle the issue, scaling-factors or R-factors are used for observation error variances to adjust observation impacts for each observation. Empirically derived values of the R-factor for SLA and SST are set as 1.5 and 16, respectively, whereas for subsurface observations of temperature and salinity, an R-factor of 6 is

https://doi.org/10.5194/egusphere-2026-534
Preprint. Discussion started: 29 April 2026

chosen. The impact of observations with large standard deviations from the background is maintained by an adaptive quality control procedure (Sakov and Sandery, 2017) where observations with large innovations are penalised by setting the K-factor to 2. The ensemble spread is maintained by the combined effect from the static covariance and relaxation of the prior spread technique (Zhang et al., 2004) with alpha = 0.7 (Tippett et al., 2003) and capped inflation (Sakov 2014) of 2 %. Analysis produced by the data assimilation is used directly to replace the ocean model restarts. This method is found to produce better forecast performance than adaptive nudging (Sandery et al., 2011), which was used in previous OceanMAPS versions (v2.0, v2.1).

2.4 Ocean model

The ocean general circulation model used in OceanMAPSv4p1i is the Ocean Forecast Australia Model version 3 (OFAM3; Oke et al., 2008), which is a specific implementation of the Geophysical Fluid Dynamics Laboratory (GFDL) Modular Ocean Model (MOM) version 5 (MOM5.0) (Griffies, 2012). OFAM has been continuously developed over Bluelink projects 1 and 2 (Brassington et al., 2007; Oke et al., 2008; Oke et al., 2013, Brassington et al., 2012). OFAM3 utilises uniform horizontal grids with a 1/10° x 1/10° resolution throughout the full model domain, covering all longitudes and latitudes between 75° S and 75° N. OFAM3 has 51 vertical levels in "zstar" coordinates. The vertical resolution is 5 m for the top 2 cells and smoothly graduates to 10m using a cosine function down to a depth of 100 m, with uniform 10m resolution down to 200 m, where three further cosine tapers are applied to coarsen the vertical resolution to a maximum bottom cell depth of 944 m and maximum model depth of 5000 m. A partial cell algorithm is applied to the “bottom” cell of each water column to improve the representation of the average bathymetry. A minimum column depth of 15 m (3 cells) is also applied. Bathymetry is based on GEBCO releases (Smith and Sandwell, 1997). The model has been implemented with bi-harmonic friction with no neutral physics parameterisations. The model employs a first-order upwind advection scheme for TKE, based on the k-ε scheme from the General Ocean Turbulence Model (GOTM; Umlauf et al., 2005) for parametrising the vertical mixing. Horizontal mixing is based on a biharmonic Smagorinsky viscosity scheme (Griffies and Hallberg, 2000). The model lacks an explicit tidal representation; however, it utilises the parametric effect of tidal mixing (Lee et al., 2006). Surface salinity is restored to monthly averaged climatology (Ridgway and Dunn, 2003), with a restoring timescale of 100 days.

2.5 Forecast System

Ocean forecast generation for each day involves a series of sequential tasks. Figure 1 shows the schematic of the OceanMAPSv4p1i forecast system. OceanMAPSv4p1i forecast system comprises five sequential tasks, namely (1) behind real-time (BRT) analysis at 3-day behind real-time using the ensemble mean and anomalies from the 1 day hindcast from the BRT analysis of the previous forecast cycle, (2) a model hindcast forward run (1-day) for all 48 ensemble members saving 24hr 3D temperature and salinity fields and 2hrly SST fields and 12hrly sea surface height fields (3) near real-time (NRT) analysis at 2-days behind real-time, (4) 2-day catch-up runs for a selection of ensemble members to bring them to real-time, and (5) forecast run that predict model states out to a lead time of 7-days. This sequential setup differs from the previous OceanMAPS (v4p0i), as the previous layout fragmented the ensemble hindcasts into batches of 16 per day over the 3 days of the analysis cycle to distribute the computational cost. The new set-up uses the equivalent computational cost (Brassington et al., 2023) to update

https://doi.org/10.5194/egusphere-2026-534
Preprint. Discussion started: 29 April 2026

all 48 ensemble members for the 1-day cycle. Similar to the previous version, the system generates three individual member forecasts (run001-003) and one average member (run004) 7-day forecasts daily. The run004 initial condition is based on the average of all 48 analysis ensemble members rather than the average of 16 member restarts available for version 4.0i. Run-004 is the recommended forecast product as it shows the lowest mean absolute error (MAE), as noted in OceanMAPSv4p0i (Brassington et al., 2023). Unless specified otherwise, when we refer to ocean forecasts from OceanMAPSv4p0i and OceanMAPSv4p1i, it implies run004 forecasts. The run004 forecast in OceanMAPSv4p1i is constructed from the forward model runs using initial conditions created from the average NRT analysis fields. Another difference in forecast products between the previous EnKF OceanMAPS version (v4p0i) and the latest version is in the run001 forecasts. In the newest version, no flux perturbations are applied to member-001 in the analysis side (step 2 in the forecast system layout explained above), whereas all 48 members are treated the same in OceanMAPSv4p0i. This means run001 forecasts in OceanMAPSv4p1i closely resemble the deterministic forecasts in the past OceanMAPS systems (OceanMAPS3px, OceanMAPS2px) based on the EnOI approach and without the randomness seen in OceanMAPSv4p0i.

3 Performance

Daily ocean forecast outputs from a five-and-a-half-month period (August 20, 2023–January 31, 2024) parallel pre-operational deployment of OceanMAPSv4p1i are evaluated against the operational forecast products from the OceanMAPSv4p0i system. Both versions of OceanMAPS assimilate observations from the same platforms and run with the same surface flux products from the ACCESS-G3 system. Hence, any system improvements and changes can be attributed to differences in the data assimilation settings and forecast system layouts.

3.1 Forecast error time series

Time series of spatial-mean bias, MAE for the first 24-hour forecast (Day 1), and histogram of the number of observations used to calculate statistics for four prognostic variables of SST, SLA, Temperature and Salinity belonging to the global region (60° S-60° N, 180° E-180° W) are shown in Fig. 2-Fig. 5. Red lines indicate statistics belong to OceanMAPSv4p1i, and blue lines represent OceanMAPSv4p0i. All available observations in the data assimilation cycle are used to calculate forecast errors represented in these figures. SST forecast fields are compared to observations every 3 hours, SLA fields are compared to observations every 12 hours, whereas Temperature and Salinity fields are compared daily. For SST and SLA, though the match-ups are done in sub-daily time steps, errors and observation counts are consolidated into a daily value, providing a single value for straightforward interpretation. Thick lines in the time series belong to the average forecast product (run004), whereas thin lines are for individual member forecasts (member-001, run001).

Figure 2 shows the error time series for both systems' 24-hour sea surface temperature forecasts. The mean bias in SST for OceanMAPSv4p1i is close to zero and shows minimal temporal variability for both the run001 and run004 forecast products. On the other hand, OceanMAPSv4p0i bias, although hovering close to zero, shows significant variability; this is especially true for the run001 forecast. The considerable variability observed in the

https://doi.org/10.5194/egusphere-2026-534
Preprint. Discussion started: 29 April 2026

individual member forecasts (run001) from OceanMAPSv4p0i is attributed to the random flux perturbations applied to ensemble member-001 during the analysis cycle. As noted earlier, we have retained ensemble member 001 in OceanMAPSv4p1i to integrate forward without any perturbations to the original surface fluxes. This means that the SST biases observed in the single-member forecast from OceanMAPSv4p1i are very similar to those in the averaged forecasts in terms of magnitude and variability. The MAE for SST in OceanMAPSv4p1i is significantly less than OceanMAPSv4p0i. The average SST forecast MAE's from the new system is ~0.244 °C compared with ~0.265 °C for the previous operational system, an improvement close to 8% in the forecast product. Single-member SST forecasts have shown the most significant improvement compared to the previous system; OceanMAPSv4p1i's performance is on par or better than the average forecast product from OceanMAPSv4p0i. Single-member SST forecast MAE's from the previous operational system are around 0.3 °C, and OceanMAPSv4p1i errors are in the 0.26 °C ballpark, over 10 % improvement in SST forecast errors. The histogram shows that the satellite SST observations used to calculate forecast errors are approximately constant (without any significant drop in numbers) throughout the experiment period (over 4×10^6 observations per day).

The forecast error time series for sea level anomaly is shown in Fig. 3. SLA biases in OceaMAPSv4p1i are slightly better than OceanMAPSv4p0i, especially noticeable in the initial half of the experimental period. This is true for the average forecast (run004) and single-member (run001) forecasts. Similar to the time series of SST MAEs, the SLA graph also shows reduced errors for OceanMAPSv4p1i. Errors in the single-member forecast (run001) from the new system are on par or better than the average forecast (run004) from OceanMAPS4.0i. Time series have less day-to-day variability when compared to the previous operational system. Notably, the run001 forecast from OceanMAPSv4p1i is highly consistent, indicating the stability of the new system and resulting in minimal sea level corrections to model states during the data assimilation cycle. OceanMAPSv4p1i shows over 6 % improvement in SLA errors for the average forecast (run004) and over 7 % improvement for run001 compared to the previous operational system.

Forecast error time series for temperature and salinity are shown in Fig. 4 and Fig. 5. They are constructed by matching available profile observations throughout the water column. All the systems exhibit slight seasonality in temperature bias, with increased values observed by the end of October and bias decreasing during the austral summer period. However, the OceanMAPSv4p1i temperature bias is less than that of OceanMAPSv4p0i. This is true for the average (run004) and single-member (run001) forecasts. At the start of the experimental period, temperature bias hovered around 0.05 °C; by the end of January, biases were close to zero for OceanMAPSv4p1i. MAE also show decreased errors for OceanMAPSv4p1i compared to the previous version. For run004, the mean MAE for the forecast period is 0.42 °C, whereas the mean is close to 0.45 °C for OceanMAPSv4p0i. Though not as evident as the SST and SLA time series, MAE for the run001 temperature forecast also shows improvement in errors in OceanMAPSv4p1i. MAE from OceanMAPSv4p1i run001 forecast is generally seen with fewer errors throughout the time periods compared to OceanMAPSv4p0i, with peaks in errors typically less pronounced. Unlike the other three variables, the salinity bias has increased slightly for OceanMAPSv4p1i compared to OceanMAPSv4p0i, as evident in Fig. 5. Salinity errors decreased significantly in the previous system upgrade, OceanMAPSv4p0i, from OceanMAPSv3p4 (Brassington et al., 2023). In comparison, forecast salinity error

https://doi.org/10.5194/egusphere-2026-534
Preprint. Discussion started: 29 April 2026

improvements seen for the current upgrade are marginal. However, no significant degradation in salinity errors has been observed globally, with slightly fewer errors in the average forecast product.

3.2 Spatial error maps

Figures 6-9 show spatial error maps in 4°×4° spatial bins based on 24-hour forecast fields from the average forecasts (run004). Spatial error maps of single-member forecasts are not shown. The errors are constructed using 24-hour OceanMAPS forecasts matched against the CLASS-4 observation data (Ryan et al., 2015; Divakaran et al., 2015). Class-4 observations are quality-controlled and used internationally as reference observations for ocean forecast verification and intercomparison. Class-4 SST reference observations are based on drifter data. SLA reference observations are from the JASON-series satellite, whereas delayed mode quality-controlled Argo profiles are used for forecast comparisons of temperature and salinity. It should be noted here that the *in-situ* drifter observations from SST are not used in the assimilation cycle of OceanMAPS and, hence, are considered fully independent. Although both Jason and Argo data are used in the data assimilation, both have approximately a 10-day repeat cycle. With NRT analysis at 2 days behind real-time in OceanMAPSv4p1i, any information from these platforms in observation locations is considered ~12 days old system persistence.

Figure 6 shows SST spatial bin maps of SST MAE from OceanMAPSv4p0i and v4p1i. Spatial bins with less than 25 observations are omitted from the figure. Error patterns in both systems are similar, and the error range is generally within 0-1 °C. The more significant errors typically occur in high-energetic/high-variability regions and along coastal current systems. The Kuroshio, Gulf Stream, Agulhas retroflection region, and Brazil Current all show higher MAEs in OceanMAPS forecasts. SST errors are, in general, small away from the coast, especially in the centre of gyres and deep oceans, where the variability is less. Nonetheless, the difference in SST forecast errors between the systems (OceanMAPSv4p0i-OceanMAPSv4p1i) reveals that the forecasts from the latest version show a notable reduction in errors throughout the global ocean. The most significant reductions (close to/over 0.2 °C) occur in the high-energetic regions and along current systems, where OceanMAPS have high errors. There is also a marked reduction in SST forecast errors south of 40° S latitude close to the Antarctic Circumpolar Current (ACC) vicinity. There are a small number of spatial bins where OceanMAPSv4p1i errors are larger than those of OceanMAPSv4p0i. However, these differences are generally very small, and only 5-6 of the cells have shown error differences over 0.15 °C. It should also be noted that the distribution of SST errors will be affected by the period of comparison, which is approximately half of the annual cycle.

The spatial binned map of MAEs for SLA are shown in Fig. 7. OceanMAPSv4p1i and OceanMAPSv4p0i show similar spatial patterns, with significant errors concentrated on regions with known high sea surface height variability. These regions are characterised by high MAE values exceeding 10 cm and are observed in the Gulf Stream and the Kuroshio in the Northern Hemisphere. In the southern hemisphere, they are along the Agulhas retroflection, the Brazil-Malvinas confluence, the ACC, and on the East Australian coast. Unlike the SST map, several areas exhibit mid-range errors, including the Somali Current, the Leeuwin Current region, the California Current, the West Africa/Cape Verde region, the East Tropical Pacific, and the South Equatorial Current in the Indian Ocean. Outside of the areas mentioned above, SLA errors are relatively smooth and negligible. SLA error

https://doi.org/10.5194/egusphere-2026-534
Preprint. Discussion started: 29 April 2026

differences between the systems show that OceanMAPSv4p1i significantly improves forecast performance over OceanMAPSv4p0i in all regions where traditionally large SLA errors are observed. We note that OceanMAPSv4p1i errors have increased over the Baltic and Labrador seas in the northern hemisphere and the southernmost latitudes in the southern hemisphere. We acknowledge that the OFAM3 model will have deficiencies in representing these marginal seas, as it lacks explicit tides, coupled sea-ice, or a coupled wave model. Nonetheless, OFAM3 is used in both systems. The more frequent assimilation cycles indicate a systematic deterioration in performance in the aforementioned regions.

Figure 8 shows spatial errors in temperature based on quality-controlled Argo observations. The spatial maps of temperature MAE from OceanMAPS are primarily similar to SLAs, with matching locations of high eddy activity or high variability in density. These spatial errors in temperature are slightly less pronounced in high-variability regions compared with those of SLAs. It should be noted that the sample size per bin of *in situ* observations is significantly smaller, and the retention of *in situ* observations in the high-variability region is also lower. The Black Sea and the Sea of Japan are other regions with prominent temperature errors. Differences in MAEs between the systems show that most bins have reduced error, with the most significant improvements in the mid-latitudes, where the circulation includes eddies and western boundary currents. There are spatial bins where OceanMAPSv4p1i have more errors than those of OceanMAPSv4p0i. However, the magnitude of these differences in the majority of bins is found to be insignificant, except in the Baltic and Labrador seas.

Salinity forecast spatial errors are shown in Fig. 9. Unlike other variables, salinity exhibits basin-wide spatial errors of over 0.05 PSU, particularly in the Atlantic Ocean, Arabian Sea, Bay of Bengal, and the southeastern Indian Ocean. The difference in salinity errors between the systems indicates that the bulk of the model domain has reduced salinity errors in OceanMAPSv4p1i. Improvements in salinity forecasts in OceanMAPSv4p1i closely follow the trend found in temperature, with a reduction in errors observed in mid-latitudes. Furthermore, basin-wide improvements in salinity have been noticed in the South Atlantic Ocean and Arabian Sea as a result of this system upgrade.

The information in the binned maps in Fig. 6-9, along with spatial errors for single-member forecasts (un-001), is translated into a histogram for the number of positive bins (red) and negative bins (blue) for all four variables: SST, SLA, Temperature, and Salinity histograms are shown in Fig. 10. This indicates all four variables have a net gain in the run-004 forecast, with the most significant improvement found for SLA. The run-001 forecast also shows substantial improvements in SST, SLA and Temperature; salinity shows no improvement/degradation. It is worth noting that salinity has shown the most significant percentage improvement in spatial bins in the previous OceanMAPS system upgrade (Brassington et al., 2023). This indicates that of the four variables, salinity is the least impacted by latency and likely reflects the limitation of the observing system in the near surface. It is also an indication that salinity has more persistence.

3.3 Forecast error growth

Figure 11 shows the forecast lead-time MAE error analysis for SST and SLA. Two sets of graphs for each variable are presented: one based on all the available quality-controlled super-observations (mostly measured by satellite)

https://doi.org/10.5194/egusphere-2026-534
Preprint. Discussion started: 29 April 2026

used by the EnKF data assimilation system and one based on CLASS-4 reference observations. SST forecast error growth shows that errors in OceanMAPSv4p1i from the average forecast and single-member forecasts are better than forecast products from OceanMAPSv4p0i. In general, looking at the error bars, the maximum forecast MAE for v4p1i is less than the minimum MAE for v4p0i. Errors in SST are found to be growing at a faster rate with increase in forecast lead time in OceanMAPSv4p0i. However, error growth is close to linear in OceanMAPSv4p1i. In Fig. 11a the MAE difference between the systems for average forecasts is 0.0258 °C on Day 1, which increases to 0.0341 °C by Day 7. On the other hand, the SST MAE difference for the single-member forecasts is more or less steady, with 0.0362 °C on Day 1 and 0.0355 °C on Day 7. Overall, MAE and variability in SST based on CLASS-4 drifter observation comparisons in Fig. 11b are higher than those in Fig. 11a. This is due to the independence and lower sample size of SST observations from drifters compared with remotely sensed SST using satellites. The SST error difference between the systems in Fig. 11b for average forecasts on Day 1 is 0.0376 °C, reaching 0.0519 °C on Day 7, holding a steady improvement of over 12% throughout the forecast lead times. And in single-member forecasts, the difference between the systems is even greater, starting at 0.0461 °C on Day 1 and 0.0528 °C by Day 7.

Single-member SLA forecasts performance from OceanMAPSv4p1i are on par with the average forecast product from OceanMAPSv4p0i throughout forecast lead times. Figure 11c shows that for average member forecasts, OceanMAPSv4p1i MAE, compared with OceanMAPSv4p0i, is less than 0.003 m on Day 1 and 0.002 m on Day 7. Similarly, for single-member forecasts, OceanMAPSv4p1i have an improvement of 0.0035m on Day 1 and 0.0021 m on Day 7. SLA MAEs constructed using CLASS-4 Jason-3 observations (Fig. 11d) show the averaged SLA forecasts from OceanMAPSv4p1i improved by over 7 % on Day 1 and over 4 % on Day 7, compared to the previous operational system. For single-member SLA forecasts, comparing OceanMAPSv4p1i to OceanMAPSv4p0i, the MAE decreased by 8.64 % on the Day 1 forecast lead time and by 4 % on the Day 7 forecast lead time.

MAE error growth curves for temperature and salinity are shown in Fig. 12. Errors for temperature from OceanMAPSv4p1i are less than those of OceanMAPSv4p0i for average and single member forecasts, Fig. 12a-b. Temperature error growths are found to be stable throughout forecast lead times for OceanMAPSv4p1i compared to OceanMAPSv4p0i. Compared with all available *in-situ* profile observations, an MAE offset of ~0.027 °C and ~0.017 °C has been noticed between the systems for average and single-member forecasts. The magnitude of errors in temperature and salinity based on CLASS-4 quality-controlled Argo is understandably smaller than that based on all observations. Figure 12b shows that the error growth curve from OceanMAPSv4p1i single-member forecast is similar to the average member forecast from OceanMAPSv4p0i. An MAE difference of ~0.03 °C and ~0.22 °C is noticed between systems for average member (run004) and single forecasts, respectively. The salinity MAE error growth from Fig. 12c shows that the single-member forecasts from both systems are on equal footing, whereas the average forecasts show a slight improvement for OceanMAPSv4p1i. Salinity errors based on quality-controlled Argo data (Fig. 12d) reveal that MAE for both forecast products have a modest deterioration in the quality in OceanMAPSv4p1i compared to OceanMAPSv4p0i.

https://doi.org/10.5194/egusphere-2026-534
Preprint. Discussion started: 29 April 2026

3.4 Summary diagrams

The relative accuracy of both systems for the Day 1 forecast on the four variables SLA, SST, temperature, and salinity is shown using radar diagrams in Fig. 13. MAEs for each variable are normalised using values from single forecasts (run001) errors related to OceanMAPSv4p0i, which is found to have the largest errors between the products. It is evident that the average forecast product from OceanMAPSv4p1i is the most accurate on all four variables using all available observations. However, using CLASS4 observations, the quality of salinity accuracy from the average forecast products from OceanMAPSv4p1i and OceanMAPSv4p0i are similar. The second most accurate product based on comparisons from all observations is the average forecast product from OceanMAPSv4p0i. The product has comparable accuracy to that of the single-member forecast from OceanMAPSv4p1i for SST and SLA and performs better in temperature and salinity forecasts. However, using CLASS4 data, compared to OceanMAPSv4p0i average member forecasts, single member forecasts from OceanMAPSv4p1i show better relative accuracy for SST and SLA. The temperature accuracy of the single forecast product from OceanMAPSv4p1i is also similar to the average forecast product from OceanMAPSv4p0i. Despite that, salinity relative errors for OceanMAPSv4p1i run001 (member001) forecast are more significant than those of other forecast products.

Model forecasts and observed estimates are also compared using Taylor diagrams (Taylor, 2001) in Fig. 14. Taylor diagrams represent unbiased RMS error (with the mean removed) and the cross-correlation between observed and modelled estimates of an oceanic property. They also represent the standard deviation of the property considered. Taylor diagrams presented here have skill-score shading feature, as defined by Taylor (2001), which aids in interpreting results between systems based on different model resolutions and numerical methods. SST forecasts and CLASS4 observed drifter SSTs are compared in the Taylor diagram in Fig. 14a. Using RMS error as the most basic metric for evaluation, average member SST forecasts from OceanMAPSv4p1i are the closest to the observation, followed by single-member forecasts from OceanMAPSv4p1i, average member forecasts and single-member forecasts from OceanMAPSv4p0i. All systems and the observations have similar variability in SST. However, the SST correlation with observations is slightly higher for the OceanMAPSv4p1i forecast products compared with OceanMAPSv4p0i.

Figure 14b compares SLA forecasts with Jason-3 observational products. OceaMAPSV4p1i SLA from the average forecast product shows the fewest errors, high correlation and is closest to the observation in the Taylor diagram. Variability from the single-member forecasts from OceanMAPSv4pi is closest to that of the observation and has the second-lowest error and correlation among the forecast products compared. In general, OceanMAPSv4p0i forecast products lag behind OceanMAPSv4p1i in the diagram, with marginally high errors and lower correlation values. Understandably, the variability of the single-member forecasts is slightly higher than that of the average forecast products from each system and comparable to the observed variability. Temperature and salinity profile forecasts, as well as CLASS4 quality-controlled Argo profiles for depths less than 200 m, are compared in Fig. 14c-d. Similar to SST and SLA, the average forecasts for temperature from OceanMAPSv4p1i exhibit the least errors and the highest correlation with observations among the forecast products displayed. Single-member forecasts from OceanMAPSv4p1i and average forecasts from OceanMAPSv4p0i have matching errors and correlation coefficients. However, the variability from OceanMAPSv4p1i (run001) is closer to that of

https://doi.org/10.5194/egusphere-2026-534
Preprint. Discussion started: 29 April 2026

observations than that of OceanMAPSv4p0i. The upper layer (<200 m) salinity forecasts from OceanMAPSv4p1i produce the least skill among the systems, with elevated errors and decreased correlation, compared to those of OceanMAPSv4p0i products. This suggests the potential difficulty of constraining upper salinity errors with reduced subsurface salinity observations due to the 1-day observation window in the OceanMAPSv4p1i system. Except for the upper layer salinity, the single-member forecasts from OceanMAPSv4p0i are the farthest away from the observations and have the least skill in all three other variables. In a similar vein, the average forecasts from OceanMAPSv4p1i are closest to the observations and have demonstrated the highest skill among the forecast products.

4 Conclusion

The Ocean Forecast System (OceanMAPS), based on EnKF data assimilation at the Australian Bureau of Meteorology, has been upgraded by introducing a one-day BRT and NRT analysis cycle in place of the previous version's 3-day single BRT analysis cycle. This design change reduces the overall latency of the analysis. The system has completed the pre-operational stage (this paper is based on the pre-operational forecast data) and has been in operational run since June 5, 2025, at the bureau's new operational supercomputer. Similar to the previous system, the new system has 48 dynamic ensemble members; however, with the 1-day model ensemble forward run instead of the three-day run every three days in OceanMAPSv4p0i. This means the computational cost of the new system is kept effectively the same as the previous version, with negligible increments due to the introduction of additional NRT analysis. Use of NRT analysis average as forecast initial condition significantly improved mesoscale ocean eddy representation in OceanMAPSv4p1i forecasts compared to OceanMAPSv4p0i (see supplementary material). A selection of statistical results shows that the 7-day forecasts from the new system are performing robustly better when compared with the available observing systems. The most significant gains from this change are for SST and SLA, which have the fastest persistence error growth. The improvements in SST and sea level are consistent with improvements in upper-level temperature. A comparison of the new system with OceanMAPSv4p0i indicates an approximate improvement of 8-10 % in SST and 6-7 % in SLA in the average forecast (run004) product. Removing the flux perturbation from ensemble member 001, as implemented in OceanMAPSv4p1i, improved the quality of the single-member forecast (run001) compared to the previous version. On average, we found single-member forecast improvements of 10 % in SST and 7 % in SLA.. OceanMAPSv4p1i and OceanMAPSv4p0i are considered interim versions as indicated by “i” at the end of their names.

The next stage of the major upgrade for OceanMAPS (OceanMAPSv5p0) will include adopting a full-global coupled ocean and sea-ice model, based on NEMO (Nucleus for European Modelling of the Ocean; Madec and NEMO system team, 2019). This strategic shift aligns the bureau with ocean model developments at UK Met Office, facilitated through the Momentum partnership. The Global Ocean and Sea-Ice model version (GOSI9) configuration with eORCA12 (1/12-degree horizontal resolution and 75 vertical levels) and SI^3 sea ice component (Storkey et al., 2018; Blockley et al., 2024; Guiavarc'h et al., 2025), in EnKF setup through EnKF-C (Sakov, 2014) with 24 dynamic members, is showing promising results. The system is currently in the research forecast demonstration phase at the National Computing Facility (NCI), Australia.

https://doi.org/10.5194/egusphere-2026-534
Preprint. Discussion started: 29 April 2026

Code and data availability

OceanMAPS operational forecasts and parallel forecast outputs for OceanMAPSv4p1i are available from the NCI Data catalogue at https://doi.org/10.25914/pgvq-8x20. Class4 files and forecast statistics generated using EnKF-C data assimilation software are published in zenodo and are available through open access https://doi.org/10.5281/zenodo.18689166.

Author contributions

PS developed EnKF-C data assimilation software, developed and tuned ocean forecasting systems OceanMAPS v4.0i and v4.1i. GB managed the OceanMAPS project and designed the operational layout of OceanMAPS v4.0i and v4p1i. PD handled the ocean model, conducted forecast design experiments, and took the lead in transferring the system from research to operations. XH implemented the system at the Bureau machine and conducted parallel forecast runs. Writing: PD produced the data, figures and prepared the original draft.

Acknowledgement

Meteorological service agreement for operational sustainment of ocean forecast services in support of the Royal Australian Navy, 2014-2024.

The MetOp-A SST data from the Naval Oceanographic Office are made available under Multi-sensor Improved Sea Surface Temperature (MISST) project sponsorship by the Office of Naval Research (ONR). The Suomi NPP Visible Infrared Imaging Radiometer Suite (VIIRS) and NOAA-20 VIIRS data were provided by the Group of High-Resolution Sea Surface Temperature (GHRSST) and the National Oceanic and Atmospheric Administration (NOAA). GHRSST and JAXA/EORC provided the AMSR-2 SST data.

The Altimetry data are obtained from Radar Altimeter Database System (RADS) and provided by EUMETSAT/NOAA/TU Delft.

The Argo profile data were collected and made freely available by the International Argo Program and the national programs that contribute to it (https://argo.ucsd/edu). The Argo program is part of the Global Ocean Observing System. The Argo data are obtained from French and US Global Data Assembly Centres (GDACS).

GODAE OceanView/OceanPredict Intercomparison and Validation Task Team for providing CLASS-4 reference observations on SST, SLA and profiles.

https://doi.org/10.5194/egusphere-2026-534
Preprint. Discussion started: 29 April 2026

Reference

Bell, M. J., Lefèbvre, M., Le Traon, P.-Y., Smith, N., and Wilmer-Becker, K.: GODAE: The Global Ocean Data Assimilation Experiment, *Oceanography.,* 22(3),14-21, https://doi.org/10.5670/oceanog.2009.62, 2009.

Blockley, E., Fiedler, E., Ridley, J., Roberts, L., West, A., Copsey, D., Feltham, D., Graham, T., Livings, D., Rousset, C., Schroeder, D., and Vancoppenolle, M.: The sea ice component of GC5: coupling SI^3 to HadGEM3 using conductive fluxes, Geosci. Model Dev., 17, 6799–6817, https://doi.org/10.5194/gmd-17-6799-2024, 2024.

Brassington, G. B.: Multicycle ensemble forecasting of sea surface temperature. *Geophysical Research Letters*, *40*(23), pp.6191-6195, 2013

Brassington, G. B.: Forecast Errors, Goodness, and Verification in Ocean Forecasting. *Journal of Marine Research* 75, (3), 2017.

Brassington, G. B., Freeman, J., Huang, X., Pugh, T., Oke, P. R., Sandery, P. A., Taylor, A., Andreu-Burillo, I., Schiller, A., Griffin, D. A., Fiedler, R., Mansbridge, J., Beggs, H., and Spillman, C. M.: Ocean Model, Analysis and Prediction System (OceanMAPS): version 2, CAWCR Technical Report., No. 052, 110 pp, 2012.

Brassington, G. B., Oke, P. R., and Pugh, T.: BLUElink Operational Ocean prediction in Australia, Advances in Geosciences., 5, Ocean and Atmospheres (OA), Edited by: Choi, H. and. Speers, World Scientific Publishing, 87-95, https://doi.org/10.1142/9789812707215_0011, 2006.

Brassington, G. B., Pugh, T., Spillman, C., Schulz, E., Beggs, H., Schiller, A., and Oke, P. R.: BLUElink Development of operational oceanography and servicing in Australia, *Journal of Research and Practice in Information Technology., 39*, 151-164, 2007.

Brassington, G. B., Sakov, P., Divakaran, P., Saima, A., Sweeney-van, J. K., Huang, X., and Stewart, A.: OceanMAPS v4p0i: a global eddy-resolving EnKF ocean forecasting system, In Oceans 2023-Limerick IEEE., 1-8, 2023.

Bureau of Meteorology.: Implementation of OceanMAPS (Bluelink> Ocean Forecast System) (18 October 2007), Operations Bulletin., 69, http://www.bom.gov.au/australia/charts/bulletins/APOB69.pdf, 2007.

Bureau of Meteorology.: Operational Upgrades to Ocean MAPS (Bluelink> Ocean Forecast System) (8 November 2011), Operations Bulletin., 89,http://www.bom.gov.au/australia/charts/bulletins/apob89.pdf, 2011.

Bureau of Meteorology.: APS2 upgrade to the ACCESS-G Numerical Weather Prediction system (16 March 2016), Operations Bulletin., 105, http://www.bom.gov.au/australia/charts/bulletins/APOB105.pdf, 2016.

Bureau of Meteorology.: Operational Upgrade to OceanMAPS version 3 (Bluelink > Ocean Forecast System) - global ocean forecasting (April 2017), Operations Bulletin., 111, http://www.bom.gov.au/australia/charts/bulletins/apob111-external.pdf, 2017.

Bureau of Meteorology.: APS3 upgrade of the ACCESS-G/GE Numerical Weather Prediction system (20 October 2019), Operations Bulletin., 125, http://www.bom.gov.au/australia/charts/bulletins/opsbull_G3GE3_external_v3.pdf, 2019

Chamberlain, M. A., Oke, P. R., Brassington, G. B., Sandery, P., Divakaran, P., and Fiedler, A. R. S.: Multiscale data assimilation in the Bluelink ocean reanalysis (BRAN), Ocean Modelling., 166, 101849, https://doi.org/10.1016/j.ocemod.2021.101849, 2021.

https://doi.org/10.5194/egusphere-2026-534
Preprint. Discussion started: 29 April 2026

Clayton, A. M., Lorenc, A. C., and Barker, D. M.: Operational implementation of a hybrid ensemble/4D-Var global data assimilation system at the Met Office, Quart. J. Roy. Meteor. Soc., 139, 1445–1461, doi:10.1002/qj.2054, 2013.

Counillon, F., Sakov, P., and Bertino, L.: Application of a hybrid EnKF-OI to ocean forecasting, Ocean Science, 5, 389-401, doi:10.5194/os-5-389-2009, 2009.

Cummings, J., Bertino, L., Brasseur, P., Fukumori, I., Kamachi, M., Martin, M. J., Mogensen, K., Oke, P., Testut, C .E., Verron, J., and Weaver, A.: Ocean data assimilation systems for GODAE, Oceanography., 22(3), 96–109, https://doi.org/10.5670/oceanog.2009.69, 2009.

Divakaran, P., Brassington, G. B., Ryan, A. G., Regnier, C., Spindler, T., Mehra, A., Hernandez, F., Smith, G. C., Liu,Y., and Davidson, F.: GODAE OceanView Inter-comparison for the Australian Region, Journal of Operational Oceanography., 8(sup1), s112-s126, DOI:10.1080/1755876X.2015.1022333, 2015.

Dombrowsky, E., Bertino, L., Brassington, G. B., Chassingnet, E. P., Davidson, F., Hurlburt, H. E., Kamachi, M., Lee, T., Martin, M. J., Mey, S., Tonani, M.: GODAE systems in operation, Oceanography, 22(3), 80–95, https://doi.org/10.5670/oceanog.2009.68, 2009.

Evensen, G.: Sequential data assimilation with a nonlinear quasi-geostrophic model using Monte-Carlo methods to forecast error statistics, J. Geophysical Research., 99, 10143-10162, 1994.

GHRSST Science Team.: The Recommended GHRSST Data Specification (GDS)2.0, document revision 5, the GHRSST International Project Office, 123 pp, https://www.ghrsst.org/wp-content/uploads/2016/10/GDS20r5.pdf, 2012

Griffies, S. M.: Elements of MOM5, GFDL Ocean Group Technical Report No. 7., NOAA/Geophysical Fluid Laboratory, https://mom-ocean.github.io/assets/pdfs/MOM5_manual.pdf, 2012.

Griffies, S. M. and Hallberg, R. W.: Biharmonic friction with a Smagorinky-like viscosity for use in large-scale eddy-permitting ocean models. Monthly Weather Review., 128(8), 2935-2946, 2000.

Guiavarc'h, C., Storkey, D., Blaker, A. T., Blockley, E., Megann, A., Hewitt, H., Bell, M. J., Calvert, D., Copsey, D., Sinha, B., Moreton, S., Mathiot, P., and An, B.: GOSI9: UK Global Ocean and Sea Ice configurations, Geosci. Model Dev., 18, 377–403, https://doi.org/10.5194/gmd-18-377-2025, 2025.

Hernandez, F., Blockley, E., Brassington, G. B., Davidson, F., Divakaran, P., Drévillon, M., Ishizaki, S., Garcia-Sotillo, M., Hogan, P. J., Lagemaa, P., Levier, B., Martin, M., Mehra, A., Mooers, C., Ferry, N., Ryan, A., Regnier, C., Sellar, A., Smith, G. C., Sofianos, S., Spindler, T., Volpe, G., Wilkin, J., Zaron, E. D., and Zhang, A.: Recent progress in performance evaluations and near real-time assessment of operational ocean products, Journal of Operational Oceanography., 8(sup2), s221-s238, DOI: 10.1080/1755876X.2015.1050282, 2015.

Huang, X., Divakaran, P., Taylor, A., Brassington, G., Beggs, H., Zhong, A., Sakov, P., Entel, M., Charles, S., and Matthews, L.: Operational upgrade to OceanMAPS version 3.3, Operations Bulletin., 128, Bureau of Meteorology, http://web.bom.gov.au/nmoc/stan/opsbull/opsbull-128.pdf, 2020.

Huang, X., Divakaran, P., Sakov, P., Brassington, G. B., Henrichs, J., Beggs, H., Aijaz, S., Entel, M., Zhong, A., Sanders C., Oke, P., Chamberlain, M., Fielder, R., and Taylor A.: Operational upgrade to OceanMAPS version 3.4, Operations Bulletin., 134, Bureau of Meteorology, http://web.bom.gov.au/nmoc/stan/opsbull/opsbull-134.pdf, 2021.

IGST (International GODAE Steering Team).: The Global Ocean Data Assimilation Experiment Strategic Plan, GODAE Report., 6, 2000.

Kilpatrick, K. A., Podestà, G. P., and Evans, R.: Overview of the NOAA/NASA advanced very high resolution radiometer Pathfinder algorithm for sea surface temperature and associated matchup database, Journal Of Geophysical Research., 106, 9179-9197, 10.1029/1999JC000065, 2001.

https://doi.org/10.5194/egusphere-2026-534
Preprint. Discussion started: 29 April 2026

Large, W. G. and Yeager, S. G.: Diurnal to decadal global forcing for oceans and sea-ice models: the data sets and flux climatologies, NCAR Technical Note, 112 pp, 2004.

Lee, H. C., Rosati, A., and Spelman, M.J.: Barotropic tidal mixing effects in a coupled climate model: oceanic conditions in the Northern Atlantic, Ocean Modelling., 11, 464-477, 2006.

Li, Y. and Toumi, R.: A balanced Kalman Filter ocean data assimilation system with application to the South Australian Sea, Ocean Modelling., 116, 10.1016/j.ocemod.2017.06.007, 2017.

Madec, G. and NEMO system team: Nemo Ocean Engine – version 4.0.1, Notes du Pôle de modélisation de l'Institut Pierre-Simon Laplace (IPSL), 27, Zenodo, https://doi.org/10.5281/zenodo.3878122, 2019.

Manizza, M., Le Quere, C., Watson, A. J., and Buitenhuis, E. T.: Bio-optical feedbacks among phytoplankton, upper ocean physics and sea-ice in a global model, Geophys. Res. Let., 32, L05603, doi:10.1029/2004GL020778, 2005.

Moltmann, T., Turton, J., Zhang, H-M., Nolan, G., Gouldman, C., Griesbauer, L., Willis, Z., Piniella, Á. M., Barrell, S., Andersson, E., Gallage, C., Charpentier, E., Belbeoch, M., Poli, P., Rea, A., Burger, E. F, Legler, D. M., Lumpkin, R., Meinig, C., O'Brien, K., Saha, K., Sutton, A., Zhang, D., and Zhang, Y.: A Global Ocean Observing System (GOOS), Delivered Through Enhanced Collaboration Across Regions, Communities, and New Technologies. *Front. Mar. Sci.,* 6, 291, doi: 10.3389/fmars.2019.00291, 2019.

Nowlin Jr, W. D., Smith, N., Needler, G., Taylor, P. K., Weller, R., Schmitt, R., Merlivat, L., Vézina, A., Alexiou, A., McPhaden, M., and Wakatsuchi, M.: An Ocean Observing System for Climate, Bulletin of the Americal Meteorological Society., 77 (10), 2243-2273. https://doi.org/10.1175/1520-0477(1996)077<2243:AOOSFC>2.0.CO;2, 1996.

Oke, P. R., Brassington, G. B., Griffin, D. A., and Schiller, A.: The Bluelink ocean data assimilation system (BODAS), Ocean Modelling., 21, 46-70, doi:10.1016/j.ocemod.2007.11.002, 2008.

Oke, P. R., Brassington, G. B., Griffin, D. A., and Schiller, A.: Ocean data assimilation: a case for ensemble optimal interpolation, Australian Meteorological and Oceanographic Journal., 59, 67-76, 2010.

Oke, P. R., Griffin, D. A., Schiller, A., Matear, R. J., Fiedler, R., Mansbridge, J., Lenton, A., Cahill, M., Chamberlain, M.A., and Ridgway, K.: Evaluation of a near-global eddy-resolving ocean model. Geoscientific model development., 6(3), 591-615, 2013.

Pilo, G. S., Oke, P. R., Coleman, R., Rykova, T., and Ridgway, K.: Patterns of vertical velocity induced by eddy distortion in an ocean model, Journal of Geophysical Research: Oceans., 123, 2274– 2292, https://doi.org/10.1002/2017JC013298, 2018.

Puri, K., Dietachmayer, G., Steinle, P., Dix, M., Rikus, L., Logan, L., Naughton, M., Tingwell, C., Xiao, Y., Barras, V. and Bermous, I.: Implementation of the initial ACCESS numerical weather prediction system. *Australian Meteorological and Oceanographic Journal*, *63*(2), 265-284, 2013.

Ridgway, K. R. and Dunn, J. R.: Mesoscale structure of the mean East Australian Current System and its relationship with topography, Progress in Oceanography., 56, 189-222, 2003.

Roemmich, D., Boebel, O., Desaubies, Y., Freeland, H., Kim, K., King, B., LeTraon, P.-Y., Molinari, R., Owens, W.B., Riser, S., Send, U., Takeuchi K., and Wijffels, S. : Argo: the global array of profiling floats, Observing the oceans in the 21st century., edited by Koblinsky, J. and Smith, N. R., Uniprint Pty, Ltd, Melbourne, 248-258, 2001.

Ryan, A. G., Regnier, C., Divakaran, P., Spindler, T., Mehra, A., Smith, G. C., Davidson, F., Hernandez, F., Maksymczuk, J., and Liu, Y.: GODAE OceanView Class 4 forecast verification framework: global ocean inter-comparison, Journal of Operational Oceanography., 8(sup1), s98-s111, DOI: 10.1080/1755876X.2015.1022330, 2015.

Sakov, P.: EnKF-C user guide, arXiv:1410.1233v10, 57 pp, https://arxiv.org/pdf/1410.1233v10.pdf, 2014

https://doi.org/10.5194/egusphere-2026-534
Preprint. Discussion started: 29 April 2026

Sakov, P. and Oke, P. R.: A deterministic formulation of the ensemble Kalman filter: an alternative to ensemble square root filters, Tellus., 60A, 361-371, 2008.

Sakov, P. and Sandery, P.: An adaptive quality control procedure for data assimilation, Tellus A: Dynamic Meteorology and Oceanography., 69(1), https://doi.org/10.1080/16000870.2017.1318031, 2017.

Sandery, P. A., Brassington, G. B., and Freeman, J.: Adaptive nonlinear dynamical initialization, *J. Geophys. Res.*, 116, C01021, doi:10.1029/2010JC006260, 2011.

Scharroo, R., Leuliette, E., Naeije, M., Martin-Puig, C., and Pires, N.: RADS version 4: An efficient way to analyse the multi-mission altimeter database, European Space Agency, (Special Publication) ESA SP, SP-740. https://www.scopus.com/inward/record.uri?eid=2-s2.0849884743 10&partnerID=40&md5=6e40431227e4e6d3efe9ca5fa8a16657, 2016.

Schiller, A., Brassington, G. B., Oke, P., Cahill, M., Divakaran, P., Entel, M., Freeman, J., Griffin, D., Herzfeld, M., Hoeke, R., Huang, X., Jones, E., King, E., Parker, B., Pitman, T., Rosebrock, U., Sweeney, J., Taylor, A., Thatcher, M., Woodham, R., and Zhong, A.: Bluelink ocean forecasting Australia: 15 years of operational ocean service delivery with societal, economic and environmental benefits, Journal of Operational Oceanography., 13, 1–18, https://doi.org/10.1080/1755876x.2019.1685834, 2019.

Shum, C. K., Ries, J. C., and Tapley, B. D.: The accuracy and applications of satellite altimetry, Geophysical Journal International, 121(2), 321–336, https://doi.org/10.1111/j.1365-246X.1995.tb05714.x, 1995.

Smith, N. and Lefebvre, M.: The Global Ocean Data Assimilation Experiment (GODAE). Monitoring the oceans in the 2000s: An integrated approach, International Symposium, Biarritz, 15–17 October, 1997.

Smith, W, H. and Sandwell, D. T.: Global sea floor topography from satellite altimetry and ship depth soundings, Science., 277(5334), 1956-1962, 1997.

Storkey, D., Blaker, A. T., Mathiot, P., Megann, A., Aksenov, Y., Blockley, E. W., Calvert, D., Graham, T., Hewitt, H. T., Hyder, P., Kuhlbrodt, T., Rae, J. G. L., and Sinha, B.: UK Global Ocean GO6 and GO7: a traceable hierarchy of model resolutions, Geosci. Model Dev., 11, 3187–3213, https://doi.org/10.5194/gmd-11-3187-2018, 2018.

Taylor, K. E.: Summarizing multiple aspects of model performance in a single diagram, J Geophys Res., 106, 7183-7192, 2001.

Tippett, M. K., Anderson, J. L., Bishop, C. H., Hamill, T. M., and Whitaker J. S.: Ensemble square root filters, Monthly Weather Review., 131, 1485-1490, 2003.

Umlauf, L., Burchard, H., and Bolding, K.: GOTM: source code and test case documentation: version 3.2, Marine Science Reports., 231 pp, https://www.io-warnemuende.de/files/forschung/meereswissenschaftliche-berichte/mebe63_2005-gotm.pdf, 2005.

Walters, D., Boutle, I., Brooks, M., Melvin, T., Stratton, R., Vosper, S., Wells, H., Williams, K., Wood, N., Allen, T., Bushell, A., Copsey, D., Earnshaw, P., Edwards, J., Gross, M., Hardiman, S., Harris, C., Heming, J., Klingaman, N., Levine, R., Manners, J., Martin, G., Milton, S., Mittermaier, M., Morcrette, C., Riddick, T., Roberts, M., Sanchez, C., Selwood, P., Stirling, A., Smith, C., Suri, D., Tennant, W., Vidale, P. L., Wilkinson, J., Willett, M., Woolnough, S., and Xavier, P.: The Met Office Unified Model Global Atmosphere 6.0/6.1 and JULES Global Land 6.0/6.1 configurations, Geosci. Model Dev., 10, 1487–1520, https://doi.org/10.5194/gmd-10-1487-2017, 2017.

Zhang, F., Snyder, C., and Sun, J.: Impacts of Initial estimate and Observation availability on convective-scale data assimilation with an ensemble Kalman filter. Monthly Weather Review., 132, 1238-1253, https://doi.org/10.1175/1520-0493(2004)132<1238:IOIEAO>2.0.CO;2, 2004.

https://doi.org/10.5194/egusphere-2026-534
Preprint. Discussion started: 29 April 2026

Atmospheric flux variable	Scale of randomness
Surface air temperature	0.001
Net short-wave radiation	0.075
Precipitation rate	0.15
Specific humidity	0.075
Surface winds (u10 and v10)	0.05
Downward long-wave radiation	none

Table 1: Randomness scale for atmospheric input flux variables.

https://doi.org/10.5194/egusphere-2026-534
Preprint. Discussion started: 29 April 2026

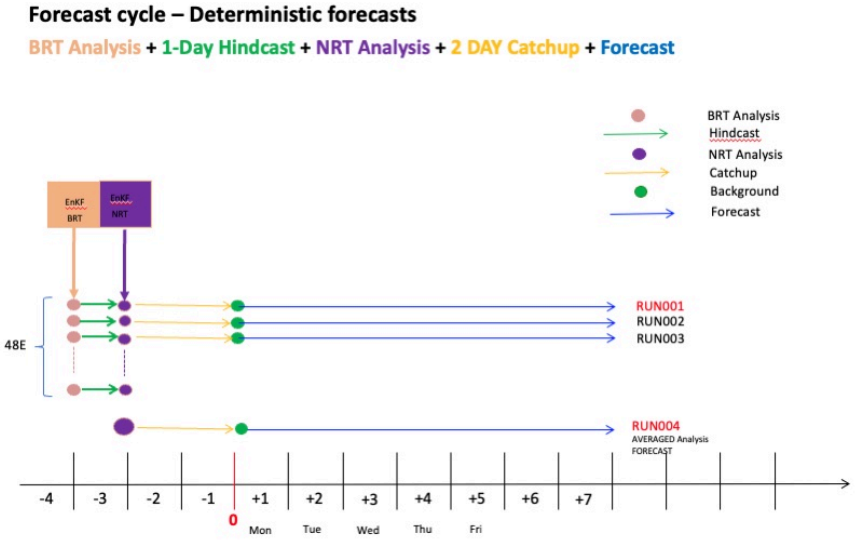

Figure 1: Schematic of the forecast system for OceanMAPSv4p1i.

https://doi.org/10.5194/egusphere-2026-534
Preprint. Discussion started: 29 April 2026

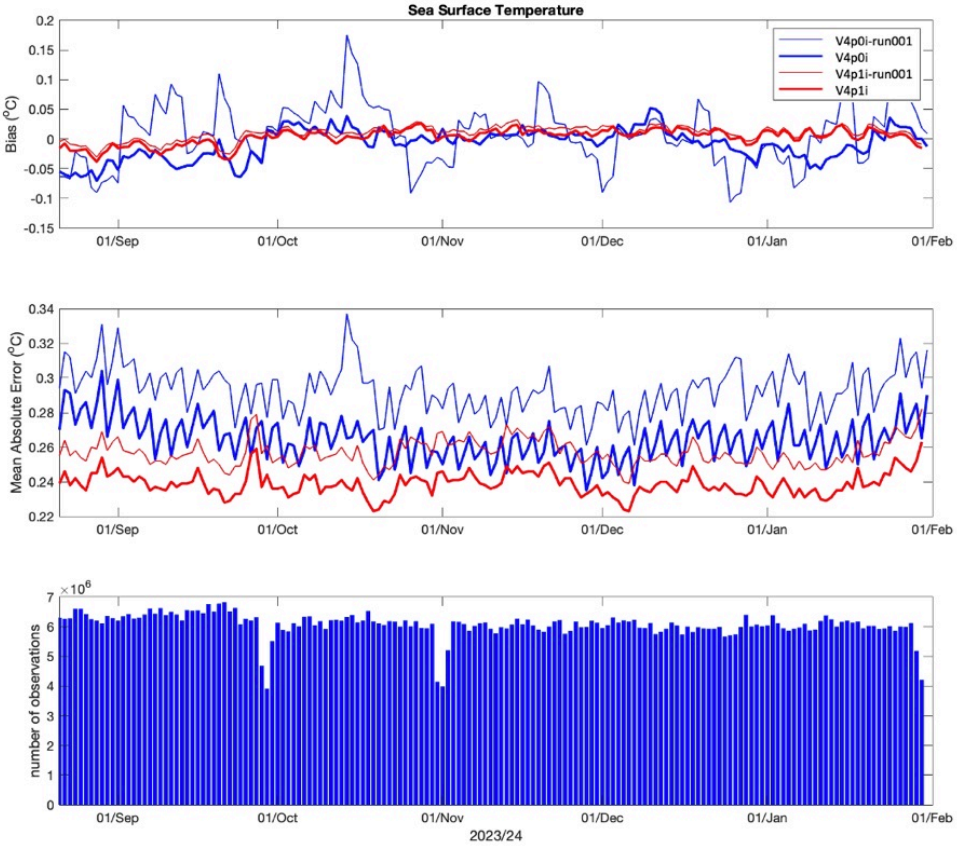

Figure 2: Area averaged time-series of SST 24-hr forecast BIAS (top), Mean Absolute Error (middle), histogram of daily SST observations (bottom); red line represents OceanMAPSv4p1i and Blue line for OceanMAPSv4p0i, thick line represent average forecasts and thin line represents one-member (deterministic) forecasts.

https://doi.org/10.5194/egusphere-2026-534
Preprint. Discussion started: 29 April 2026

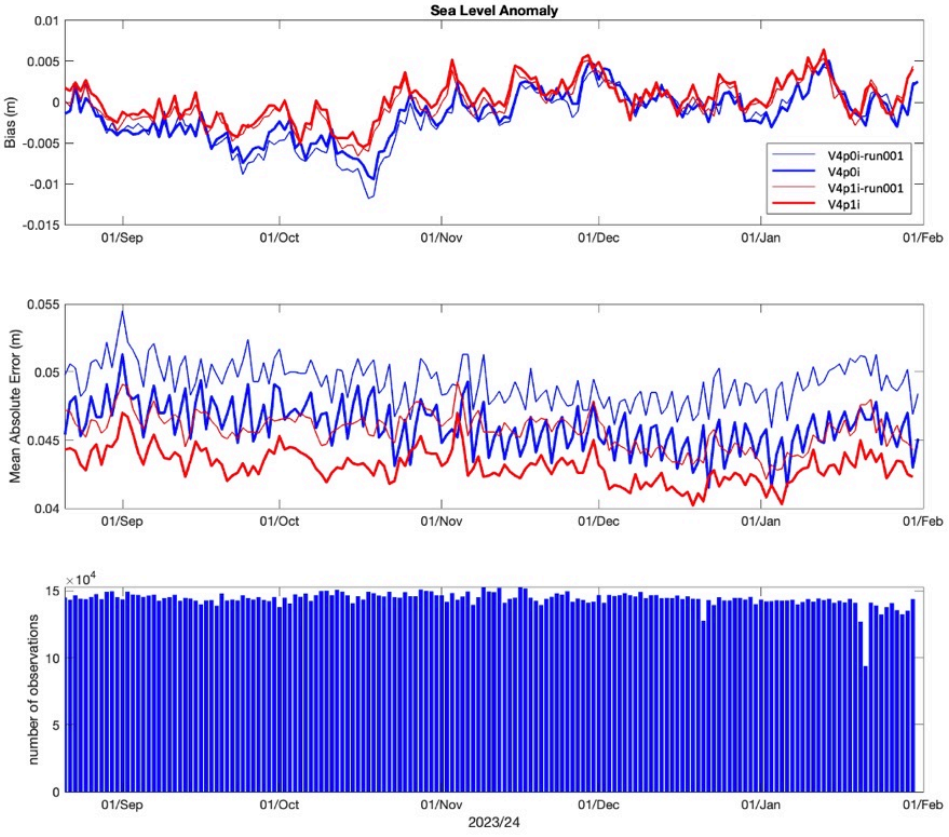

875
876 **Figure 3: Area averaged time-series of SLA 24-hr forecast BIAS (top), Mean Absolute Error (middle), histogram of**
877 **daily SLA observations (bottom); the red line represents OceanMAPSv4p1i and Blue line for OceanMAPSv40i, thick**
878 **line represents average forecasts and the thin line represents one-member (deterministic) forecasts.**

879

https://doi.org/10.5194/egusphere-2026-534
Preprint. Discussion started: 29 April 2026

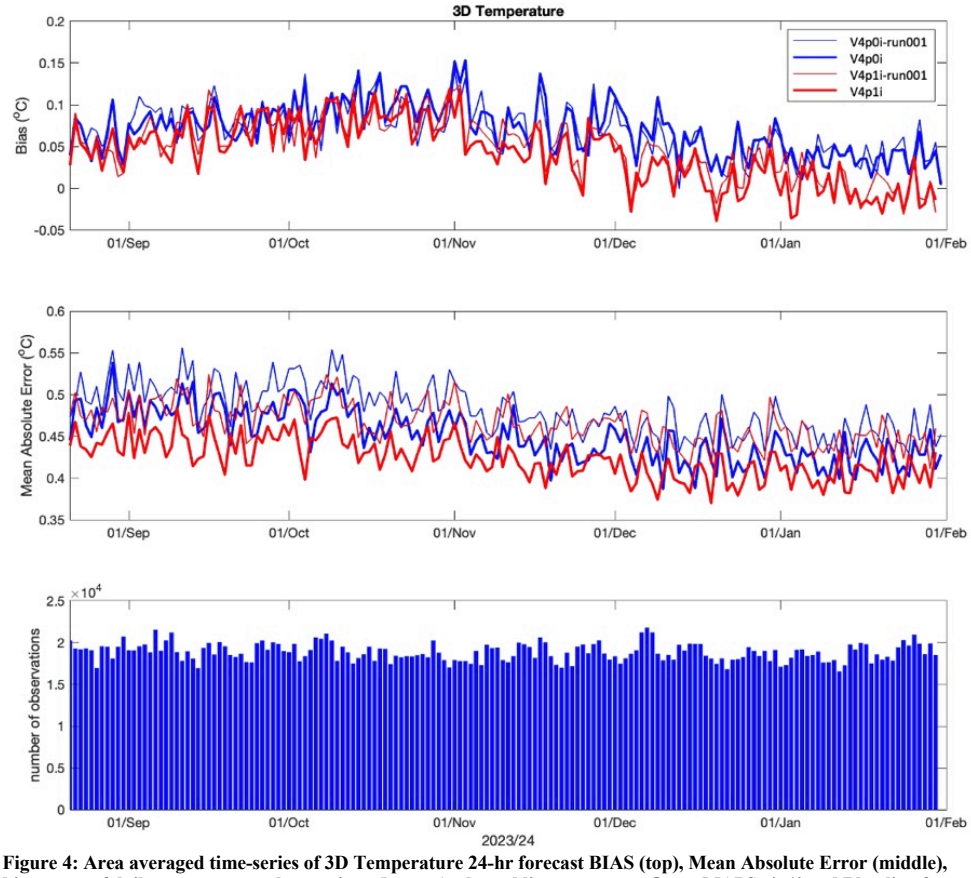

Figure 4: Area averaged time-series of 3D Temperature 24-hr forecast BIAS (top), Mean Absolute Error (middle), histogram of daily temperature observations (bottom); the red line represents OceanMAPSv4p1i and Blue line for OceanMAPSv40i, thick line represents average forecasts and the thin line represents one-member (deterministic) forecasts.

https://doi.org/10.5194/egusphere-2026-534
Preprint. Discussion started: 29 April 2026

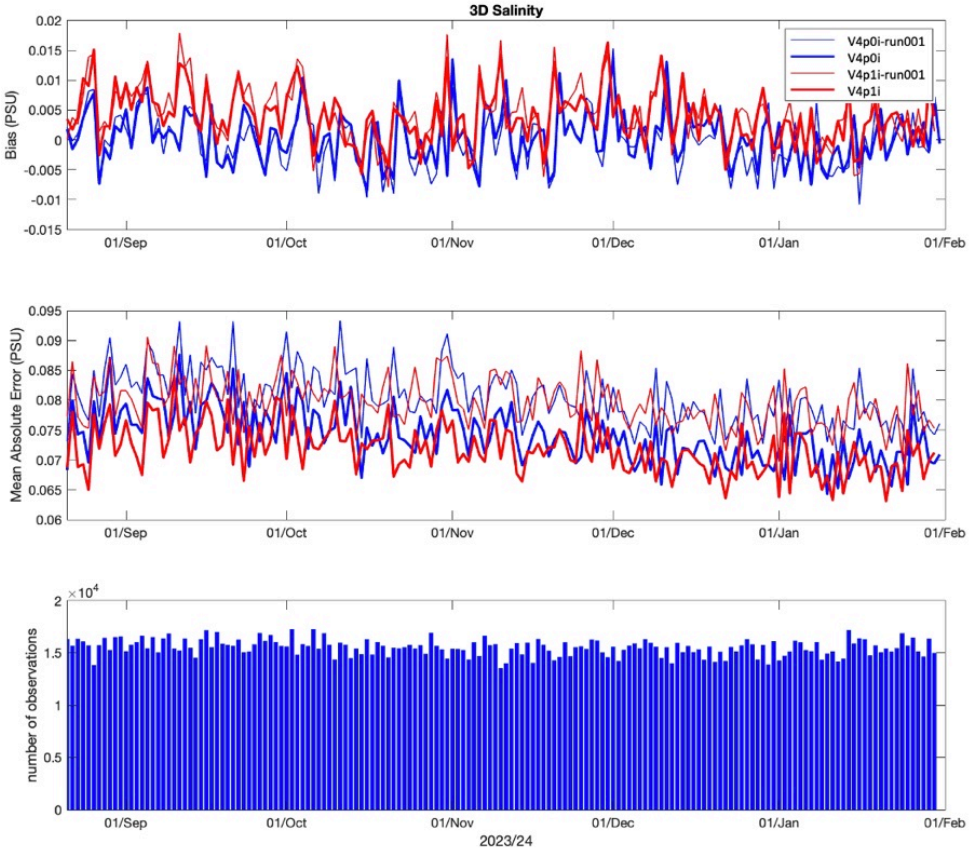

Figure 5: Area averaged time-series of 3D Salinity 24-hr forecast BIAS (top), Mean Absolute Error (middle), histogram of daily Salinity observations (bottom); the red line represents OceanMAPSv4p1i and Blue line for OceanMAPSv40i, thick line represents average forecasts and the thin line represents one-member (deterministic) forecasts.

https://doi.org/10.5194/egusphere-2026-534
Preprint. Discussion started: 29 April 2026

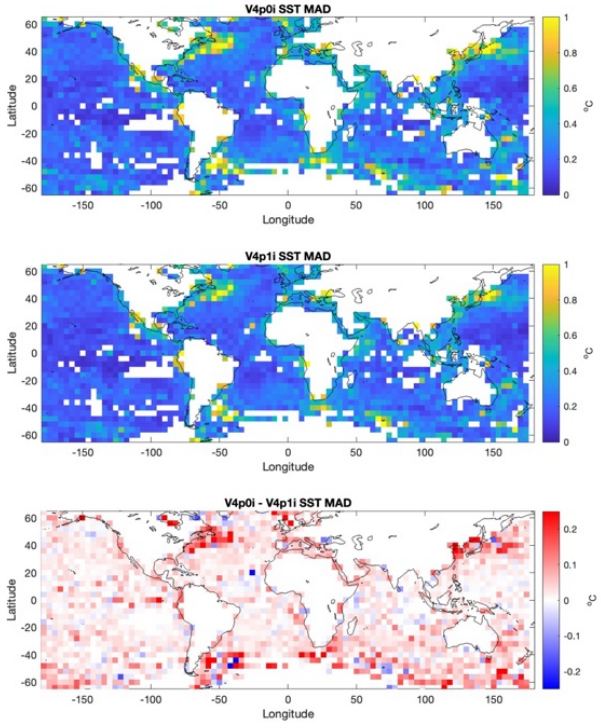

892
893 **Figure 6: SST Mean absolute error in 4° spatial bin for v4p0i(top), v4p1i(middle) and difference in MAD between v4p0i**
894 **and v4p1i(bottom), based on SST drifter observations and averaged restart products from each system. Bins with <25**
895 **observations are omitted to reduce sampling error.**

896

https://doi.org/10.5194/egusphere-2026-534
Preprint. Discussion started: 29 April 2026

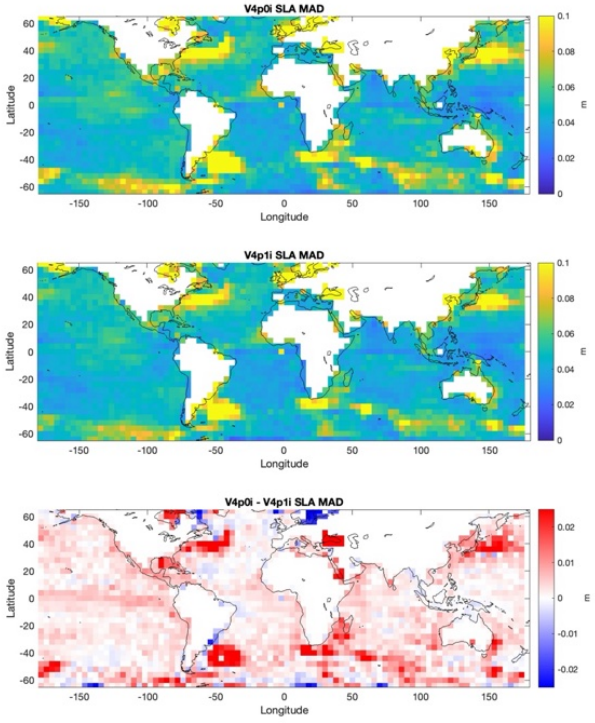

Figure 7: SLA Mean absolute error in 4° spatial bin for v4p0i(top), v4p1i(middle) and difference in MAD between v4p0i and v4p1i(bottom), based on SLA Jason-3 observations and averaged restart products from each system. Bins with <25 observations are omitted to reduce sampling error.

https://doi.org/10.5194/egusphere-2026-534
Preprint. Discussion started: 29 April 2026

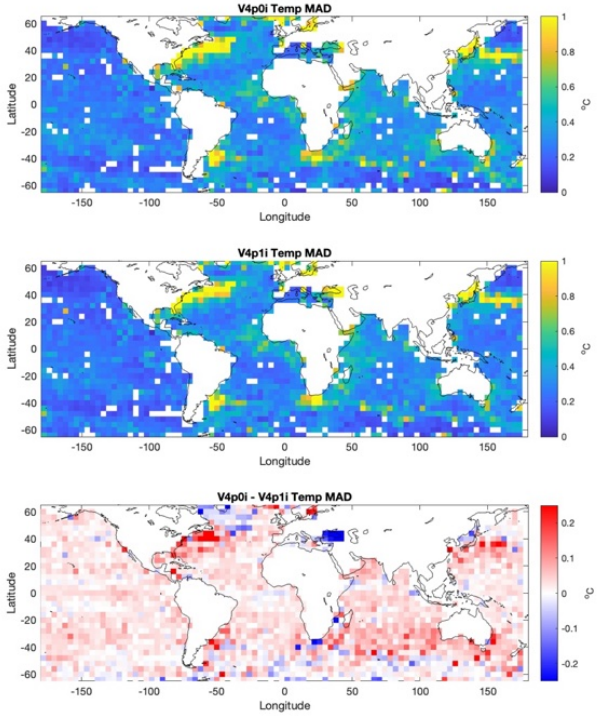

Figure 8: 3D Temperature mean absolute error in 4° spatial bin for v4p0i(top), v4p1i(middle) and difference in MAD between v4p0i and v4p1i(bottom), based on Argo temperature observations and averaged restart products from each system. Bins with <200 observations are omitted to reduce sampling error.

https://doi.org/10.5194/egusphere-2026-534
Preprint. Discussion started: 29 April 2026

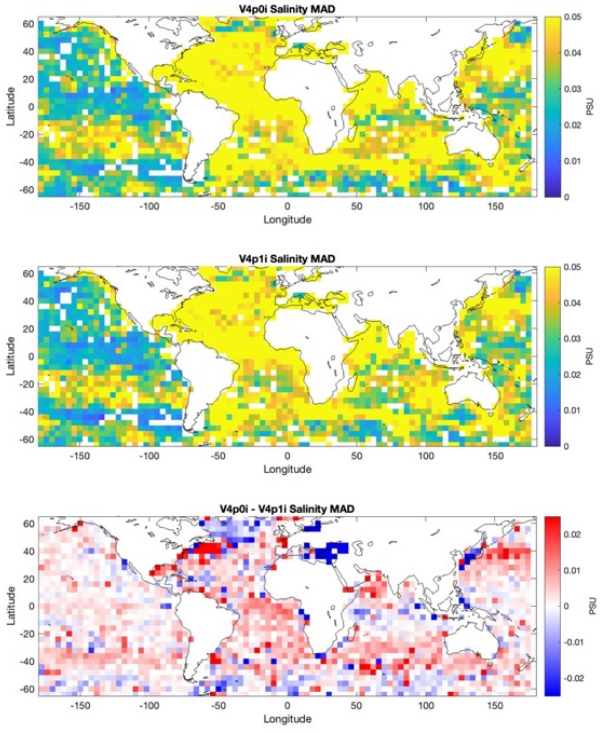

Figure 9: 3D Salinity mean absolute error in 4° spatial bin for v4p0i(top), v4p1i(middle) and difference in MAD between v4p0i and v4p1i(bottom), based on Argo salinity observations and averaged restart products from each system. Bins with <200 observations are omitted to reduce sampling error.

https://doi.org/10.5194/egusphere-2026-534
Preprint. Discussion started: 29 April 2026

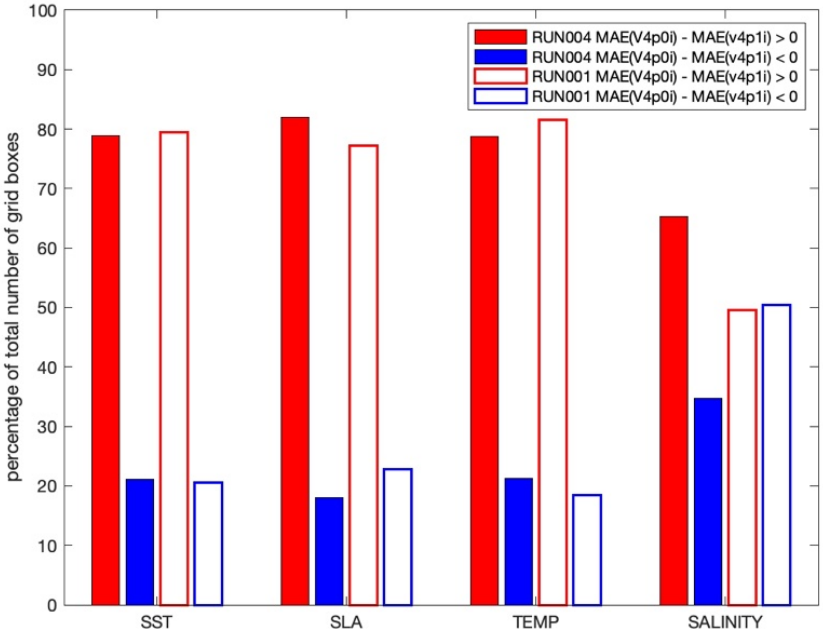

Figure 10: Percentage of positive and negative bins from the global MAE difference binned maps for all four variables.

https://doi.org/10.5194/egusphere-2026-534
Preprint. Discussion started: 29 April 2026

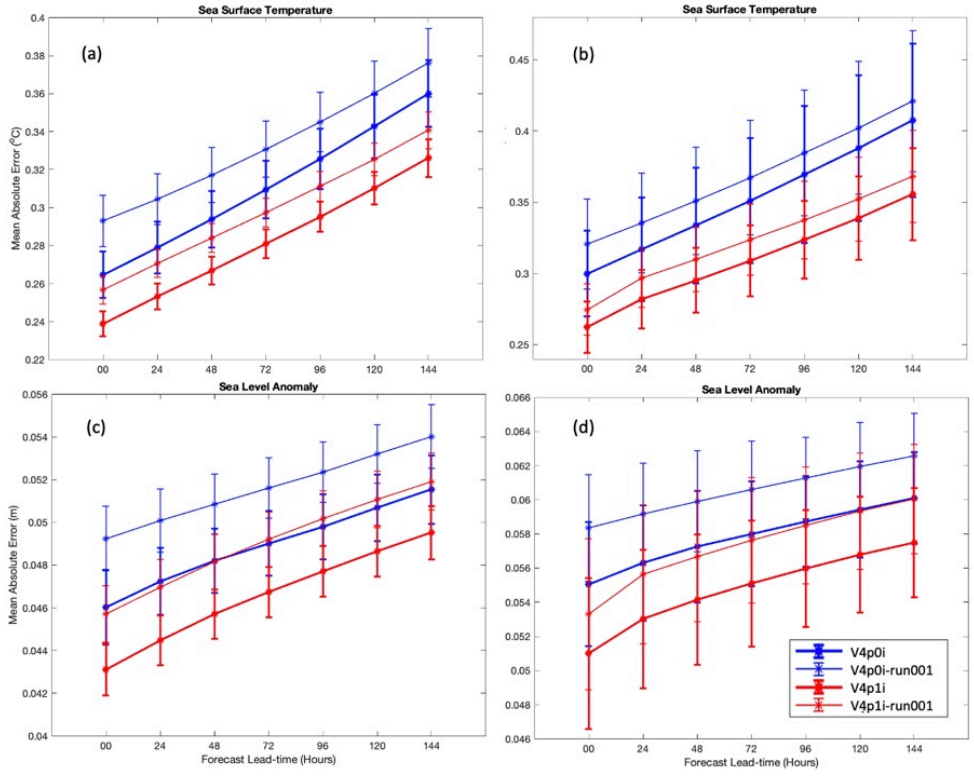

Figure 11: Lead-time forecast SST and SLA mean absolute error (a) using all available SST satellite observations, (b) using SST drifter observations, (c) using all available SLA satellite observations, and (d) using SLA Jason3 data; the red line represents OceanMAPSv4p1i and Blue line for OceanMAPSv4p0i, thick line represents average restart forecasts and the thin line represents one-member (deterministic) forecasts.

https://doi.org/10.5194/egusphere-2026-534
Preprint. Discussion started: 29 April 2026

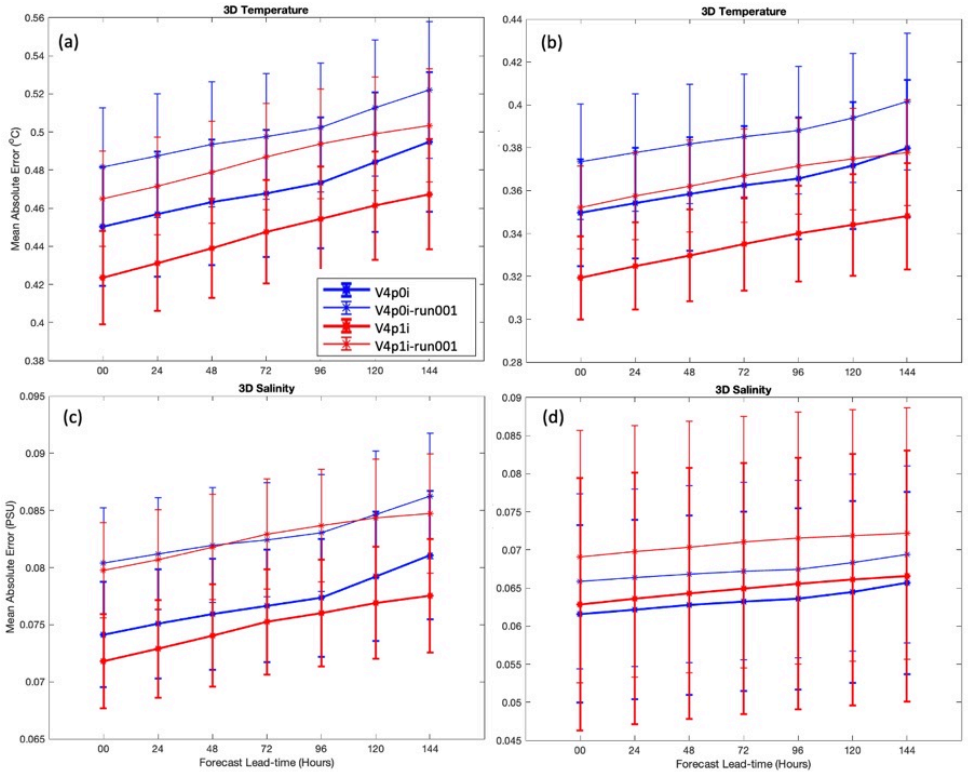

Figure 12: Lead-time forecast Temperature and Salinity mean absolute error (a) using all available temperature profile observations, (b) using class4 quality controlled delayed mode Argo temperature data, (c) using all available salinity profile observations, and (d) using class4 quality controlled delayed mode Argo salinity data; the red line represents OceanMAPSv4p1i and Blue line for OceanMAPSv4p0i, thick line represents average restart forecasts and the thin line represents one-member (deterministic) forecasts.

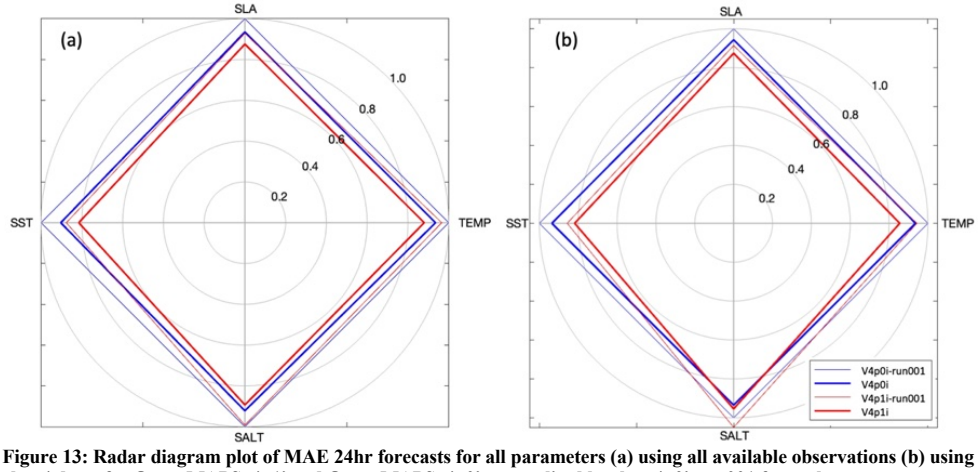

Figure 13: Radar diagram plot of MAE 24hr forecasts for all parameters (a) using all available observations (b) using class4 data; for OceanMAPSv4p1i and OceanMAPSv4p0i, normalised by the v4p0i-run001 for each parameter.

https://doi.org/10.5194/egusphere-2026-534
Preprint. Discussion started: 29 April 2026

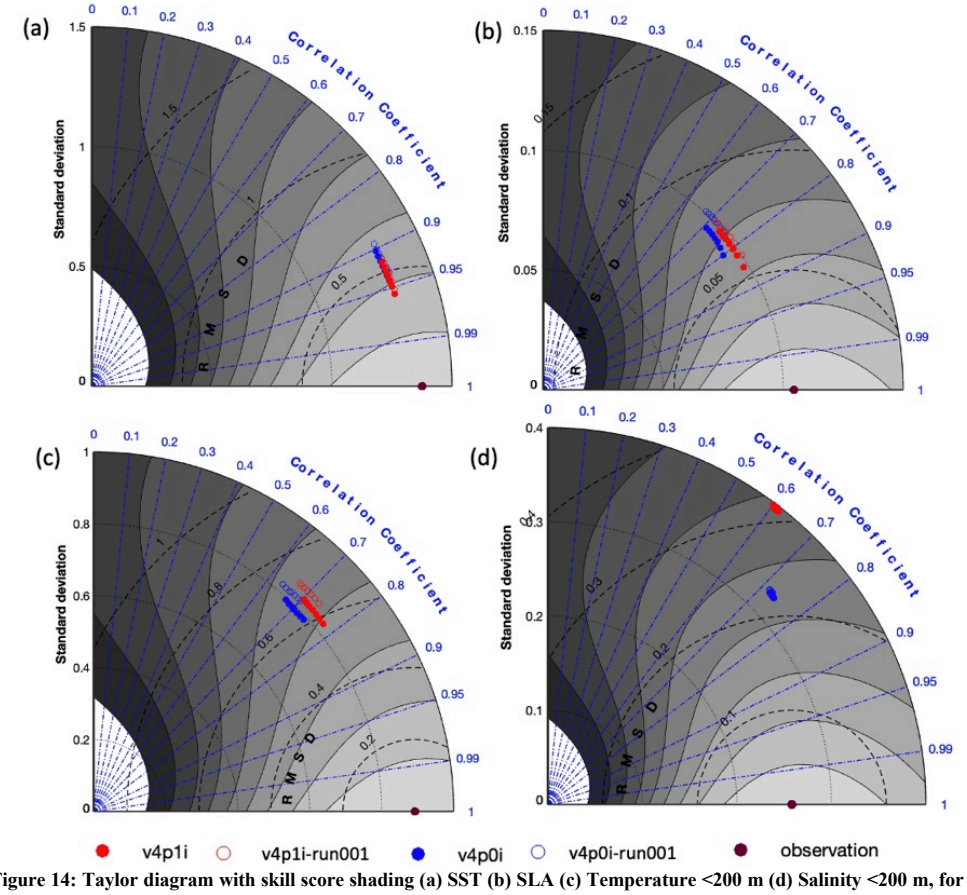

Figure 14: Taylor diagram with skill score shading (a) SST (b) SLA (c) Temperature <200 m (d) Salinity <200 m, for OceanMAPSv4p1i and OceanMAPSv4p0i forecasts.